communications materials

REVIEW ARTICLE

https://doi.org/10.1038/s43246-023-00348-5 OPEN

Development and challenges in perovskite scintillators for high-resolution imaging and timing applications

Arie Wibowo[1], Md Abdul Kuddus Sheikh[2], Lina Jaya Diguna[3], Muhammad Bagas Ananda[1], Maradhana Agung Marsudi[4], Arramel Arramel[5], Shuwen Zeng[6], Liang Jie Wong[7,8] & Muhammad Danang Birowosuto[2]✉

Inorganic scintillators play a major role in ionizing radiation detection due to their high versatility to detect multiple radiation sources such as X-rays, gamma-rays, alpha, beta, and neutron particles, and their fast and high light yield, making them especially convenient for imaging, spectroscopy, and timing applications. Scintillators-based detection systems are found, among various applications, in medical imaging, homeland security, high-energy physics, industrial control, oil drilling explorations, and energy management. This Review discusses advances and prospects of perovskite scintillators, particularly low-dimensional hybrid organic-inorganic perovskite crystals and all-inorganic perovskite nanocrystals. We highlight the promise of two-dimensional lithium-doped $(PEA)_2PbBr_4$ crystals and $CsPbBr_3$ nanocrystals as scintillators with high light yields, exceeding 20 photons/keV, and fast decay times of less than 15 ns. Such a combination may result in fast-spectral X-ray imaging, an output count rate exceeding 30 Mcps/pixel in photon-counting computed tomography, and coincidence timing resolution of less than 100 ps in positron emission tomography. We review recent strategies to further improve light yield, decay time, and coincidence timing resolution through light-matter interactions such as extraction efficiency enhancement and Purcell-enhanced scintillators. These advancements in light yields and decay times of perovskite scintillators will be particularly useful in the medical and security applications.

Recently, high-energy photons such as X- and gamma-rays have attracted great attention in modern diagnostic tools, due to their deep penetration ability[1]. Conventional detectors (X-rays conversion into electrons) based on semiconductors can be used to detect these photons, but optimizing the thickness can be a problem as for collecting the charge carries, one need relatively thin micrometer samples but this thickness is not enough to absorb high-energy radiations close to 1 MeV[2]. In this context, indirect detectors based on scintillators are more attractive as a simple, efficient, and reliable detector because scintillators can convert high-energy photons such as X- and gamma-rays and alpha, beta, and neutron particles to ultraviolet-visible

[1] Materials Science and Engineering Research Group, Faculty of Mechanical and Aerospace Engineering, Institut Teknologi Bandung, Jl. Ganesha 10, 40132 Bandung, Indonesia. [2] Łukasiewicz Research Network—PORT Polish Center for Technology Development, Stabłowicka 147, 54-066 Wrocław, Poland. [3] Department of Renewable Energy Engineering, Universitas Prasetiya Mulya, Kavling Edutown I.1, Jl. BSD Raya Utama, BSD City, Tangerang 15339, Indonesia. [4] Graduate School of Life Science, Hokkaido University, Kita-21 Nishi-11, Kita-ku, Sapporo 001-0021, Japan. [5] Nano Center Indonesia, Jalan Raya PUSPIPTEK, South Tangerang, Banten 15314, Indonesia. [6] Light, Nanomaterials & Nanotechnologies (L2n), CNRS-ERL 7004, Université de Technologie de Troyes, 10000 Troyes, France. [7] School of Electrical and Electronic Engineering, Nanyang Technological University, 50 Nanyang Avenue, Singapore 639798, Singapore. [8] CNRS-International-NTU-THALES Research Alliance (CINTRA), Nanyang Technological University, 50 Nanyang Drive, Singapore 637553, Singapore. ✉email: muhammad.birowosuto@port.lukasiewicz.gov.pl

photon emission[3,4]. Due to this unique characteristics, scintillators play a crucial role in ionizing radiation detection systems for medical imaging[5], homeland security[6], high-energy physics[7], industrial control[8], oil drilling explorations[9], and energy conversion[10].

Lanthanide scintillators are one favorable class of inorganic scintillators for fast detection and imaging applications due to their high light yield (>10 photons/keV) and fast decay times (15–60 ns). However, applications are hindered by their high price due to utilization of rare-earth elements and high temperature process for crystal-growth. Some lanthanides perovskites with cubic structure can be grown at slightly lower temperature (800-1055 K) and lower cost than other inorganic scintillators, but they are still using oven furnace[11]. On the other hand, oxide scintillators such as $LuAlO_3$ demonstrated fast decay time of 18 ns, however, this advantage is accompanied by low light output and significantly slower component[12]. In 2002, Shibuya et. al., found that $(C_6H_{13}NH_3)_2PbI_4$, a hybrid organic-inorganic perovskite (HOIP) crystal, could be used as a scintillator[13]. This finding is attractive because HOIP can be fabricated by low temperature solution-based processes. Surprisingly, HOIP investigation have shown few progress within the past 14 years, before it was restarted by the discovery of HOIP scintillators with light yield record (up to 200 photons/keV)[14]. Then, all-inorganic perovskites gained interest due to their higher densities for stopping radiations[15]. In the case of two-dimensional HOIPs, Xie and coworkers[16] tabulated several classes of two-dimensional HOIPs in which Z_{eff} vary from 30 to 40 that could be potentially useful for this purpose.

Massive developments on new perovskite scintillators could reduce the production cost up to fifty times than that of lanthanide scintillators, with higher light yields (>20 photons/keV) and faster decay times (<15 ns) than lanthanide scintillators. However, further enhancement of perovskite scintillators was still desired for their better performance on future application e.g. fast-spectral X-ray imaging, photon-counting computed tomography (PCCT), time-of-flight (TOF), positron emission tomography (PET), quantum sensing, and fusion energy[3]. For fast-spectral X-ray imaging with excellent spatial resolution, one needs at least photon flux of 10 MHz/pixel for generating spectroscopy information in each channel and such technology is not possible with 1-μs decay time of commercial microcolumn CsI:Tl X-ray imaging scintillator[3]. Similar for PCCT, output count rate (OCR) of 10 Mcps/pixel is also not enough to beat the current standard of 30 Mcps/pixel for high-flux CdTe/CZT[3]. Thus, the combination of perovskite light yields and decay times may increase the photon flux >30 MHz/pixel or OCR > 30 Mcps/pixel. This combination also may contribute to the coincidence time resolution (CTR) of PET < 100 ps[17,18].

The light yield, decay times and tunability improvement can be further pursued via light-matter interactions by tuning the formation of micro- and nano-structuring processes. The utilization of whisker and eutectic microcolumns in scintillators have been shown to be useful for high resolution in X-ray imaging via optical waveguiding effect or photonic crystal structures toward enhancement of the extraction efficiencies[19,20]. Furthermore, enhancement of scintillator properties due to the Purcell effect can be leveraged by nano-structuring the scintillator[3,21]. For instance, the Purcell effect has been theoretically proposed to enhance the scintillation decay time, resulting in an improvement of the CTR of PET from a few hundred ps to the vicinity of 30 ps[17]. In high-energy physics experiments, time resolution better than 30 ps is also needed for exploring new physics through excellent discrimination of long-live charged particles[3]. This review will focus on highlighting current issues of perovskite scintillators toward their application in spectroscopy and timing. Thus, recent strategies to improve light yield, decay time, OCR, and CTR of perovskite scintillators and related to the development of new perovskites materials and Purcell-enhanced scintillators will be further highlighted. Detailed properties and comparison with other types of scintillators are beyond the scope of this review, and have recently been summarized by Maddalena et al. in another work[22].

Low-dimensional perovskite crystal scintillators

Two-, one-, and zero-dimensional perovskite materials have attracted much interest as scintillator materials due to the light yield enhancements they benefit from as a result of quantum confinement. The research started from HOIPs[14] and progressed to all-inorganic perovskites crystals that focusing on lead-free crystals[5,23–26]. Recently, low-dimensional perovskites are attracted interest due to their high binding energy (hundreds of MeV), which enhances the exciton intensity and excitonic recombination profile, hence increasing the theoretical luminescence and faster decay time of the two-dimensional HOIP crystals[27,28]. Even though two-dimensional perovskite scintillators have crystal growth issue at this stage, current progresses demonstrated that two-dimensional perovskite can be used for large area solar cells (100 cm^2)[29]. Xie et al. also demonstrated that two-dimensional perovskite scintillators crystals with size of $1 \times 0.7 \times 0.2$ cm^3 can be prepared for wide-range radiation detection[28].

Moreover, two-dimensional HOIP can generate thermal enhancement and humidity stability due to the high hydrophobicity of the long-chain organic cation[30]. At extremely low temperature (10 K), methylammonium lead halide crystals such as $MAPbBr_3$ and $MAPbI_3$ can generate an intense peak at 770 and 540 nm with exceptional light yields of 152 and 296 photons/keV, respectively. Meanwhile, the spectrum of two-dimensional layered 2,2-(ethylenedioxy)bis(ethylammonium) lead chloride ($(EDBE)PbCl_4$) comprises a much broader band with a peak at ~520 nm (Fig. 1a)[14]. However, the two-dimensional HOIP has shown higher light yield (9 photons/keV) than the 3D perovskite (1 photons/keV) at room temperature (300 K) due to its enormous exciton-binding energy (about 360 meV)[31–33], which gives rise to a pronounced excitonic absorption below the band-edge. This result suggests the existence of giant oscillator strength that arises in two-dimensional HOIPs compared to their 3D counterparts, which is also observed for other perovskites[34]. This provides good resistance against thermal quenching at room temperature[14]. The decay time of about 10 ns from $(EDBE)PbCl_4$ is significantly faster than those of Ce^{3+}-doped $LaBr_3$ (15 ns)[35] and Ce^{3+}-doped LuI_3 (33 ns)[36]. However, $(EDBE)PbCl_4$ has afterglows of few seconds larger than those both lanthanide crystals at 10 K but they are still much less in comparison with oxide scintillators[14].

Besides $(EDBE)PbCl_4$, there are some other two-dimensional HOIP scintillators. Kishimoto et al. first implemented $(PEA)_2PbBr_4$ for a scintillator agent with light yield of 10 photons/keV[37]. The library of two-dimensional HOIP as scintillator materials was improved by Xie et al. in which the differences of scintillation properties between Ruddlesden-Popper and Dion-Jacobson types are outlined[16]. Subsequently, Ruddlesden-Popper two-dimensional HOIP crystals (including $(PEA)_2PbBr_4$) show no afterglow and thermoluminescence trap in comparison those of Dion-Jacobson crystals (including $(EDBE)PbCl_4$)[16]. However, Dion-Jacobson crystals show large stokes shift (>50 nm) in comparison to those Ruddlesden-Popper crystal due to small polaron[38], preventing the crystal from self-absorption. Then, the same group improved the scintillation properties of

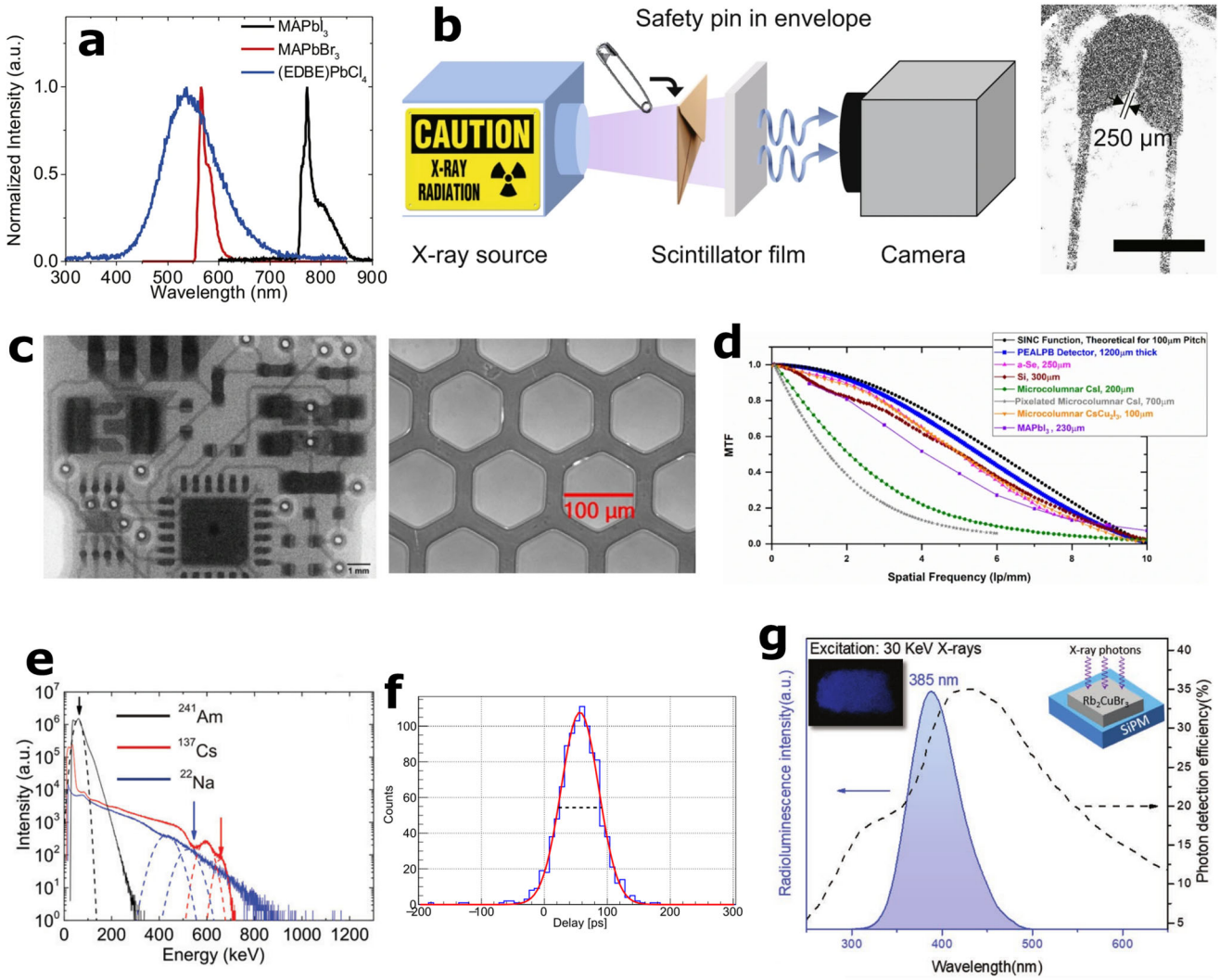

Fig. 1 Development of low-dimensional perovskite crystal scintillators. a Comparison of the normalized X-ray excited luminescence spectra at T = 10 K. **b** Scheme of X-ray imaging setup using 1:1 Li-$(PEA)_2PbBr_4$ as scintillator. The safety pin is inside the envelope and the image is shown in the right side. **c** X-ray images of a Universal Serial Bus-drive circuit and micropillar plates. **d** MTF curve of lithium-alloyed phenethylammonium lead bromide detectors along with other state-of-the-art detectors with relatively lower thicknesses. The plot thicknesses are representative of the sensor thickness levels. The sync function plot corresponding to a 100 μm pixel pitch is also shown for reference. **e** Pulse height spectra under gamma-ray excitation with different sources for Li-doped $(PEA)_2PbBr_4$ and the respective average light yields and average energy resolutions of three measurements for different energies. **f** Delay distributions at 20 mV of Li-doped $(PEA)_2PbBr_4$. The red solid lines are the Gaussian functions, which fit the distributions, and the black dotted lines provide the full width half maximum (FWHM) of the distributions. **g** Radioluminescence spectrum under 30 keV X-ray excitation and wavelength dependent photon detection efficiency of the silicon photomultiplier. The left inset shows the photograph of Rb_2CuBr_3 crystals under X-ray irradiation and the schematic model at the right shows the test method of measuring emission intensity by silicon photomultiplier. (**a**) adapted with permission from ref. [14], Copyright Springer-Nature, 2016; (**b**) adapted with permission from ref. [28], Copyright Springer-Nature, 2020; (**c**, **d**) adapted with permission from ref. [41], Copyright Springer-Nature, 2021; (**e**) adapted with permission from ref. [39], Copyright Royal Society of Chemistry, 2021; (**f**) adapted with permission from ref. [18], Copyright AIP Publishing, 2022; (**g**) adapted with permission from ref. [25], Copyright Wiley Online Library, 2019.

Ruddlesden-Popper two-dimensional HOIP by adding lithium (Li) ions, resulting in Li-doped $(PEA)_2PbBr_4$, whose light yield is increased[28]. However, there is a tradeoff when adding Li ions onto the perovskite structure (where defect is unintentionally formed). As a result, the afterglow and traps appear but they are still considered as minor contributions in comparison to those in Dion-Jacobson crystals[28]. X-ray imaging demonstration of a safety pin using a 67 μm-thick spin-coated $(PEA)_2PbBr_4$ is shown in Fig. 1b. However, the 250-μm spatial resolution (4 line pairs per millimeter (lp/mm) at modulation transfer function (MTF) of 0.2) achieved is still preliminary for X-ray imaging applications, where it is far than spatial resolutions below 100 μm (10 lp/mm at 0.2 MTF), which are routinely needed[3]. A microcolumn array was introduced by Maddalena et al.[39] to improve the resolution than that of film due to optical waveguiding effect as it was demonstrated by CsI:Tl[3] and $GdAlO_3$:Ce eutectic scintillator fibers[40]. The best spatial resolution to date of 8.8 lp/mm at 0.2 MTF was recorded by Datta et al. few months later[41], see Fig. 1c, d. However, for low dimensional HOIP crystals, the best spatial resolution of 15.7 lp/mm was reported for $(TPP)_2MnBr_4$ microcolumns[20]. Although the light yield was claimed to be 78 photons/keV[15], this scintillator has a 265-μs slow decay time limiting the applications for ultrafast X-ray imaging or spectral microcolumn functionalities[3].

Photoelectric peaks with different gamma-ray excitations that are suitable for spectroscopy have also been demonstrated with

Li-doped $(PEA)_2PbBr_4$[39]. As shown in Fig. 1e, the obtained light yield from Li-doped $(PEA)_2PbBr_4$ using gamma-ray (Cs-137) at 662 keV is around 23 photons/keV with the record of 7.7% resolution[39]. The average energy resolution displays notable improvement to 9.5% at 662 KeV compared to its undoped counterpart (11.2%). Those energy resolution values are comparable to 6–11% in NaI:Tl scintillator[3]. The higher light yield obtained from gamma-ray excitation with Li-doping confirmed that the previous bright X-ray intensity for imaging with Li-doped $(PEA)_2PbBr_4$ film[18,28]. Since the crystal can be enriched ^6Li[6], therefore it is applicable for neutron spectroscopy[28]. The ^6Li enrichment from 7.59% (concentration in natural Li precursor) to 95% in the Li-doped $(PEA)_2PbBr_4$ crystal with 1:1 Li/Pb precursor ratio, leads to the enhanced theoretical thermal neutron detection efficiency maximum from 0.4% to 4.8%, which is potential for neutron spectroscopy[28]. Thermal neutron detection is based on the neutron capture by ^6Li isotope though the following nuclear reaction: ${}_3{}^6Li + n \rightarrow {}_1{}^3H + \alpha$, and the two ionizing particles produced of ${}_1{}^3H$ and alpha have a total kinetic energy of 4.8 MeV[42]. However, the thermal neutron scintillation light yield and peak resolution of Li-doped $(PEA)_2PbBr_4$ are not as good as those shown by Cs_2LiYCl_6:0.1% Ce^{3+} of 70000 ph/n and 5.5%[43] and by Rb_2LiYBr_6:0.5% Ce^{3+} of 83000 ph/n and 5.4%[42], respectively. Recent study on Li-doped $(PEA)_2PbBr_4$ scintillator exhibits a CTR of 84 ps, due to a combination of light yield of 20 photons/keV and decay time of 15 ns, which is useful for TOF-PET, see Fig. 1f[18]. It is noteworthy to look the other two-dimensional HOIP crystals such as $(BA)_2PbBr_4$, as it even shows better light yield of 40 photons/keV and faster scintillation decay time of <8 ns than those of Li-doped $(PEA)_2PbBr_4$[39]. Sure, those properties can be much more attractive for imaging and timing applications.

Even though many reports have shown that solution-processable perovskites are promising, the presence of toxic element such as lead is potentially harmful to the environment, although some toxic elements already known in the scintillation industries as they know how to encapsulate and to manage the waste of scintillators, e.g. even cadmium scintillators are exist nowadays[44,45]. However, more research still has been directed to achieve appropriate perovskites with nontoxic properties and outstanding scintillation light yield toward radiations[5,23–26]. Yang et al. utilized a lead-free halide Rb_2CuBr_3 perovskite harnessed X-ray and UV light excitation acquired from the radioluminescence spectrum in Fig. 1g[25]. The combination between Rb_2CuBr_3 perovskite and silicon photomultiplier produces high light yield of 91 photons/keV. However, the exciton lifetime of this perovskite is tedious (41.4 μs) and not suitable for fast timing applications[25]. In addition, $Cs_3Cu_2I_5$ crystals[46] have been reported with a decay time of 51 ns (4% only, the rest is 1 μs)[5,23–26,47,48]. However, this value is still far from competing with PEA_2PbBr_4 and beyond our discussion of scintillators below 15 ns. Indeed, the lifetime of lead-free perovskites is relatively long, and future work should focus on designing fast response time scintillators with high light yield[3,21].

Perovskite nanocrystals scintillators

As mentioned in the previous two sections, unoptimized light yield (far from its theoretical value), and relatively long decay time (especially for lead-free crystals) are currently the main problems hindering perovskite scintillators toward real-world applications. In this context, perovskite scintillators in the nano-size regiments have emerged as a promising class of material for scintillators. Initial reports indicate favorable performance relative to its bulk perovskite counterparts. Although the common approach is to utilize nanostructured perovskite scintillators (i.e., bulk perovskite scintillators that undergo nano-structuring), this approach may have limitations depending on the specific choice of method, including multi-steps fabrication process, unintentional defects during patterning, or mass production[49,50]. In contrast, perovskite nanocrystals offer low cost, high yield, and easily scalable process due to it being solution processable in low temperature. The quantum confinement effect is promoted to increase the light yield of a given scintillator, while also offers a tunable wavelength emission depending on the nanocrystal size[51]. Due to the presence of heavy atoms, perovskite structured crystals are expected to have strong radiation absorption, and thus counterbalance the most glaring weakness of traditional group II-VI nanocrystals (i.e., low stopping power), while still retaining most of its strength (i.e., tunable emission, ultrafast scintillation, and high efficiency).

Chen et al. reported all-inorganic perovskites of $CsPbBr_3$ (CPB) nanocrystals and their responses to X-ray irradiation (Fig. 2a, b)[15]. Room temperature solution-processable CPB bulk crystals are tunable in terms of emission, strong X-ray absorption, and intense radioluminescence at visible wavelength, making it a very attractive material for scintillators. As nanocrystals, their absorption will be less than single crystals since they need to be mixed with polymer. The group reported imaging resolution of 2 lp/mm at 0.72 MTF, which is still much lower than CsI:Tl with microcolumn structure (100 lp/mm at 0.1 MTF)[52]. Later, this resolution was improved by Maddalena et al., as they demonstrated 4 lp/mm at 0.2 MTF[53].

Another benefit of using nanocrystals instead of single crystals is that they can increase the light yield of a scintillator through quantum confinement[15]. CPB nanocrystal scintillators have managed to achieve light yield as high as 24 photons/keV[54], which is a major improvement compared to less than 1 photons/keV in bulk single crystal CPB at room temperature[55]. There is still room for further improvements, as nanocrystals have extremely high theoretical limit of light yield due to the small band-gap of perovskites[56]. Aside from CPB, there are also other emerging nanocrystals such as $FAPbBr_3$ and $CsPbI_3$[15,54]. Unfortunately, their light yields of around a few photons/keV are much lower in comparison with that of CPB nanocrystals. There are attempts to bring lower dimension nanocrystals such as $Cs_3Cu_2I_5$ which results in a considerable light yield of 79 photon/keV, although the decay time of 1.9 μs is still slower than 1 μs of CsI:Tl[57]. Different approach than that of nanocrystals, an X-ray imaging spatial resolution of 17 lp/mm at 0.2 MTF was recorded for $Cs_3Cu_2I_5$ film with faster decay time of 1 μs[58].

An interesting recent concept in biomedical science was proposed by Ryu et al.[59]. A double encapsulation of CPB nanocrystals using SiO_2 is successfully increased the scintillator's moisture stability and prevented aggregation (Fig. 2c)[59]. The concept is to use CPB nanocrystals to attenuate X-ray, thus low-radiation X-ray imaging can be used to detect cancers non-invasively in the deep body region. Excellent moisture stability becomes a necessity since human body has a lot of water content. Presently, we still rely on fluorescence emission-based techniques, which has limited penetration depth; or high-radiation CT-scan that is harmful to healthy tissues[60]. By adhering cancer-targeting antibodies on the nanoparticles' surface, the scintillator nanoparticles will actively target and accumulate in the tumor cells, causing the tumor sites to glow bright when exposed to low-dose of X-ray (~0.1 mSv, similar to a chest X-ray) due to the attenuating property. However, although they were protected by SiO_2, the in-situ tissue imaging technique of CPB nanocrystals with lead contents may result in additional harm due to their

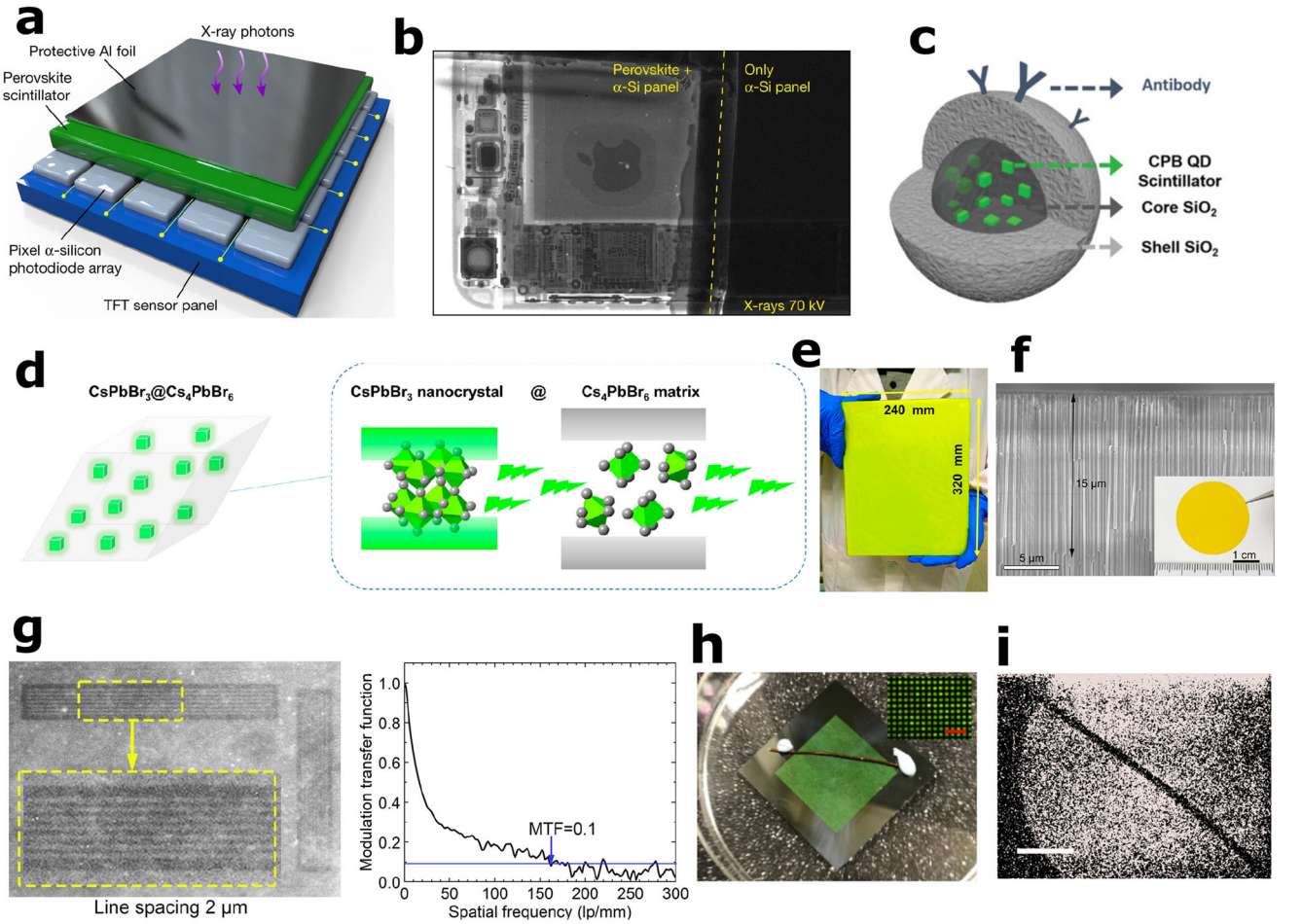

Fig. 2 Development of perovskite nanocrystals scintillators. a Design of the flat-panel X-ray imaging system consisting of 75 μm thick CPB nanocrystal thin film. **b** Comparison of X-ray image of an iPhone acquired with the CPB nanocrystal scintillator deposited on an α-Si photodiode panel (left) and bare α-Si photodiode panel (right). **c** Schematic illustration of CPB-SiO_2@SiO_2-antibody core/shell structure. **d** Schematic diagram of CPB nanocrystals embedded in Cs_4PbBr_6 matrix, and the schematic diagram of band gap of both 0D and 3D perovskites. **e** Large-area film of CPB@Cs_4PbBr_6 facile made by low-cost blade-coating process. **f** Cross-sectional SEM image showing uniform nanowire length of ~15 μm, while the inset shows picture of as-grown scintillator. **g** X-ray image of a Japan Inspection Instruments Manufacturers' Association test pattern, taken with CPB NWs/AAO scintillator (X-ray: 45 kV, 1 mA, 0.7 Gy_{air}/h). The right image shows its MTF of the imaging by slant-edge method. **h** Image of 2.5 × 2.5 × 0.1 cm silicon substrate with a 1.5 × 1.5 × 0.1 cm micro-hole pattern filled with CPB nanocrystals. A copper wire was fixed on the substrate. The inset shows a microscopy image of the filled template under UV light (scale bar = 400 μm). **i** X-ray imaging of the copper wire using CPB nanocrystals micro-hole-filled substrate shown in **i** (scale bar = 5 mm). (**a**, **b**) adapted with permission from ref. [15], Copyright Springer-Nature, 2018; (**c**) adapted with permission from ref. [59], Copyright Wiley Online Library, 2021; (**d**, **e**) adapted with permission from ref. [62], Copyright American Chemical Society, 2020; (**f**, **g**) adapted with permission from ref. [19], (**h**, **i**) adapted with permission from ref. [54], Copyright American Chemical Society, 2022.

toxicity. Looking on its application as imaging screen, thermal and photostability of nanocrystals against X-ray irradiation are often a problem, given the stability of its polymer matrix. Replacing the polymer matrix with borate glass matrix results in good thermal stability (88% of initial intensity retained after 25–300 °C heating-cooling cycle)[61]. While it shows similar photostability with polymer-blended CPB nanocrystals, annealing above its glass transition temperature can reverse the damage generated by high-intensity X-ray, showcasing its reusability potential. Nevertheless, its light yield (quantum efficiency of ~20%) is much lower than typical polymer-blended system due to defects and low atomic number of the glass matrix component.

Advancement in scintillator energy transfer mechanism is aimed to shorten decay time, obtain excellent spatial resolution, and enhance output yield. To shorten the decay time, Cao et al. introduced a strategy of perovskite nanocrystals formation in a matrix (CPB nanocrystals inside Cs_4PbBr_6 host) to improve its stability with very fast decay time of ~3 ns (Fig. 2d, e)[2,62]. Confinement by metal-organic frameworks can further hasten the response time as fast as 2.16 ns[63], making it ideal for dynamic and fast-response real-time X-ray imaging and PCCT. However, the best imaging resolution was demonstrated by CPB polymer-ceramic solution with 12.5 lp/mm at 0.2 MTF[64]. Further imaging resolution can be pushed out by incorporating the nanocrystals into pixelated scintillation screen with micropillar structure. The light is confined into a single direction and minimized the lateral propagation (60 and 160 lp/mm at 0.2 and 0.1 MTF, respectively) in CPB micropillar array in anodized aluminum oxide membrane (Fig. 2f, g)[19]. Microcolumn structure, as used in the previous crystal, can be used to avoid crosstalk in the photodetection which will lessen the spatial resolution. Another example was demonstrated by Maddalena et al. using silicon-hole template as shown in Fig. 2h where each pixel shows separate emission, consequently resulting in high imaging resolution (Fig. 2i)[54].

Despite of high photon yield and fast response time, there are some theoretical drawbacks for the nanocrystal scintillators. Nanocrystals are not single crystals, thus having more inhomogeneities compared to single crystals, making them not suitable for gamma spectroscopy as this effect generates broadening in photopeak from the pulse height spectra measurement[54]. The small Stokes shift of nanocrystals will lead to strong self-absorption, and they also have more afterglow compared to two-dimensional HOIP crystals[54]. Indeed, the concept introduced for CPB nanocrystals inside Cs_4PbBr_6 host in Fig. 2d–f was claimed to decrease the self-absorption as it was an analogous to the concept of scintillators with ion doping[47]. However, the wavelength shift of emission and absorption spectra were not observed in the other experiments[65] and therefore, the only method to reduce the self-absorption is by making the sample thickness comparable to the attenuation length at the respective deposited energy[65]. For 50 keV, all-inorganic perovskites crystals need thicknesses between 0.2 and 0.5 mm[19–22], while HOIP crystals need thicker samples of 1 mm[27,28]. For TOF-PET, CPB nanocrystals can be used as sensitizer for heterostructure configuration with high-density-but-slow scintillator through energy sharing[66]. Moreover, these nanocrystals exhibited minimum reabsorption losses from light propagation measurement under X-ray excitation, thus, enabling the detection of high-energy photons[66].

For Purcell-enhanced scintillators, perovskite materials are promising due to high quantum efficiency, fast lifetime and their emission tunability[14]. Moreover, the capability to fabricate high quality nanostructures in solution-processed perovskite is the effective means for targeted light manipulation. Two-dimensional photonic crystals such as $CsPbBr_{2.75}I_{0.25}$ (Fig. 3g) exhibited the inhibition of spontaneous light emission and redistribution of light energy[73]. Compared to the un-patterned perovskite film, the perovskite photonic crystals with different lattice constants show the photoluminescence intensity enhancement (Fig. 3h). Even though the reported results of photonic engineering in perovskite materials are mainly demonstrated for the properties under light excitation, the observed enhancement may affect their scintillation properties. Further investigation is required to demonstrate the Purcell-enhanced perovskite photonic crystals under scintillation excitation of high-energy X-ray or gamma-ray. Recently, some recent works on perovskite metasurfaces can also be used for scintillator applications to enhance the functionalities in signal processing for imaging and spectroscopy, for instance, polarization tunability[74], chirality[75], and Rashba effect[76]. For scintillation light, one should consider optimizing the perovskite structure aiming to achieve high yield radiation efficiently as well as thin enough to confine the ionized electrons and emitted photons.

Further improvements through photonic engineering

High light yield and fast decay time are the important characteristics of scintillator materials to improve its resolution in fast-spectral imaging for radiation detection and imaging, OCR in PCCT, and CTR in TOF-PET. These properties can be achieved via tunable light-matter interactions by shaping the light emission[67]. For the past 20 years, the investigation of light-matter interactions has focused on the light extraction efficiency, which is the scintillation process in more efficient ways. We already discussed how microcolumns and eutectic scintillator fibers can improve the resolution through the confinement of the light along the column or fiber direction in the previous chapters and that is one of examples for the improvement of extraction efficiency[3,40]. Another example is from Knapitsch et al. who reported light scattering from photonic crystals as novel approach to enhance the light output of scintillator to overcome the trapping issue of scintillation light due to their high electronic density led to large refraction index[68,69]. two-dimensional photonic crystal slabs on top of lutetium oxyorthosilicate (Lu_2SiO_5) scintillators demonstrate a 30–60% light yield improvement for the different patterned crystals, compared to an unstructured reference scintillator[69]. A theoretical work of Kurman et al. studied one-dimensional photonic crystals comprising cerium-doped lutetium yttrium oxyorthosilicate (LYSO:Ce) alternating with air (Fig. 3a)[70], leveraging Purcell effect that commonly used in lasers and single photon sources[71] to enhance the scintillator yield and decrease the lifetime[72]. The photonic crystal structure was shown not only to enable a fivefold enhancement of detectable photons with a faster emission rate (Fig. 3b), but also to enable a reduction the CTR by a factor 2.4 (Fig. 3c), thus improving the scintillation sensitivity and resolution. The recent experimental work of Roques-Carmes et al. observed the enhancement of X-ray-induced scintillation using a nanophotonic array of holes in cerium-doped yttrium aluminum garnet (YAG:Ce) scintillators[60] (Fig. 3d). The calculation and experimental results (Fig. 3e–f) show good agreement, where the scintillation from photonic crystal region (on) is higher than the un-patterned region (off). Nevertheless, the observation of Purcell-enhanced emission intensity has not been accompanied yet with the verification of fast lifetime, which remains a challenge.

Outlook

In this review, we have discussed recent progress in the advancement of various type of perovskite scintillators ranging from HOIPs and all-inorganic perovskites in different shapes and provided an overview of X- and gamma-ray scintillation properties of fast (≤15 ns) and high light yield (>20 photons/keV) perovskite scintillators versus commercial $LaBr_3$:Ce scintillator as shown in Table 1. The $LaBr_3$:Ce scintillator is widely regarded to possess the best combination of light yield, decay time, and energy resolution in one package, but can cost up to US$ 1550 for 8-cm^3 crystal[18,77]. For X-ray imaging, Li-doped $(PEA)_2PbBr_4$ apparent (8.8 lp/mm) spatial resolution at 0.2 MTF[41] for the multi-column structure in comparison with similar structure of CsI:Tl (100 lp/mm) at 0.1 MTF[52]. Thus, Li-doped $(PEA)_2PbBr_4$ offers adequate (7.7%) energy resolution on at 662 keV[39] in comparison to 2.0%[77] of $LaBr_3$:Ce. However, multicolumn CPB nanocrystals offer the best (60.0 lp/mm) spatial resolution at 0.2 MTF[19]. For gamma-ray spectroscopy, only Li-doped $(PEA)_2PbBr_4$ offers the best solution for perovskite. Nevertheless, this number is still worse than 2.0% of $LaBr_3$:Ce. The decay times for both Li-doped $(PEA)_2PbBr_4$ and CPB are faster than 15 ns of $LaBr_3$:Ce, resulting in good potential for timing applications. For CTR of PET, Li-doped $(PEA)_2PbBr_4$ shows the best CTR of 84 ps[18], which is almost comparable with 77 ps of $LaBr_3$:Ce[78]. We note that the cost for 8-cm-size Li-doped $(PEA)_2PbBr_4$ is only US$10, which is 155 times cheaper than that of $LaBr_3$:Ce[78]. Despite the remarkable progress as shown in their scintillation properties, such as light yield, spatial resolution, energy resolution, decay time, OCR, and CTR of perovskite scintillators are reviewed, the question remains how to anticipate the consequence of energy loss during the impingement of high-energy particles. It is noting that the absorption length of HOIP scintillator is still longer than that of inorganic scintillator (Table 1), but it is much better than that of organic scintillator, which is about 20 times[22]. Therefore, with the same light yield, thickness, and deposited energy, HOIP scintillator has less sensitivity in X-ray imaging in comparison to inorganic scintillator. Thus, a primary goal moving forward is to find a suitable approach for

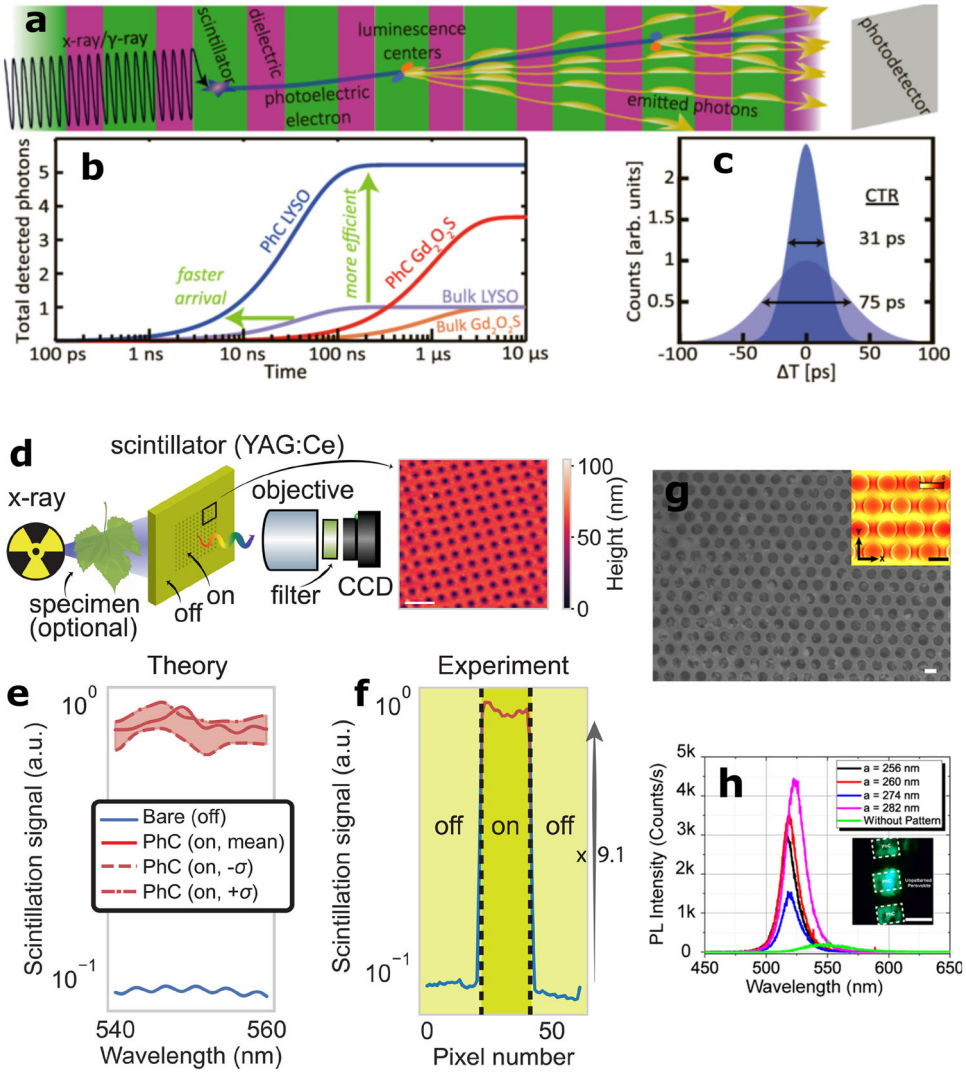

Fig. 3 Enhancement through photonic engineering. a Scintillation process of 1D photonic crystal made from the combination of scintillator material (green) with other dielectric material (pink); **b** number of detectable photons over time; and **c** coincidence time resolution (CTR) from the bulk and 1D photonic crystal scintillators. **d** X-ray scintillation experimental setup (left) and AFM image (right) of two-dimensional YAG:Ce photonic crystal scintillator; **e** calculated scintillation spectrum; and **f** measured scintillation along the line of the sample, including regions on (red) and off (blue) photonic crystal. **g** SEM image of $CsPbBr_{2.75}I_{0.25}$ perovskite two-dimensional photonic crystals and a top view of the calculated electric field distributions (inset); and **h** photoluminescence spectra of two-dimensional photonic crystals with different lattice constants and without patterns, and the sample image of photonic crystals excited by unfocused laser. (**a**–**c**) adapted with permission from ref. [70], Copyright The American Physical Society, 2020; (**d**–**f**) adapted with permission from ref. [60], Copyright The American Association for the Advancement of Science, 2022; (**g**, **h**) adapted with permission from ref. [73], Copyright American Chemical Society, 2019.

Table 1 Fast (≤15 ns) and high light yield (>20 photons/keV) perovskite scintillators versus $LaBr_3$:Ce.

		Li-doped $(PEA)_2PbBr_4$	CPB	$LaBr_3$:Ce
Absorption length, mm	@50 keV	1.17[39]	0.16*[53]	0.21[77]
	@511 keV	46.35[39]	20.06*[53]	22.75[77]
Light yield photons/keV (pulse height)		23[16]	24*[54]	78[77]
Average decay time (ns)		12.90[39]	5.97*[54]	15[77]
Energy resolution @662 keV		7.7%[39]	-	2.0%[77]
CTR (ps)		84[18]	-	77[78]
Spatial resolution @0.2 MTF (lp/mm)	Lamellar	4.0[28]	4.0*[53]/12.5**[64]	1.5[79]
	Multicolumn	8.8[41]	60.0[19]	7.3[79]

*Lamellar with 50% wt% nanocrystals[53], **Polymer-ceramics[64].

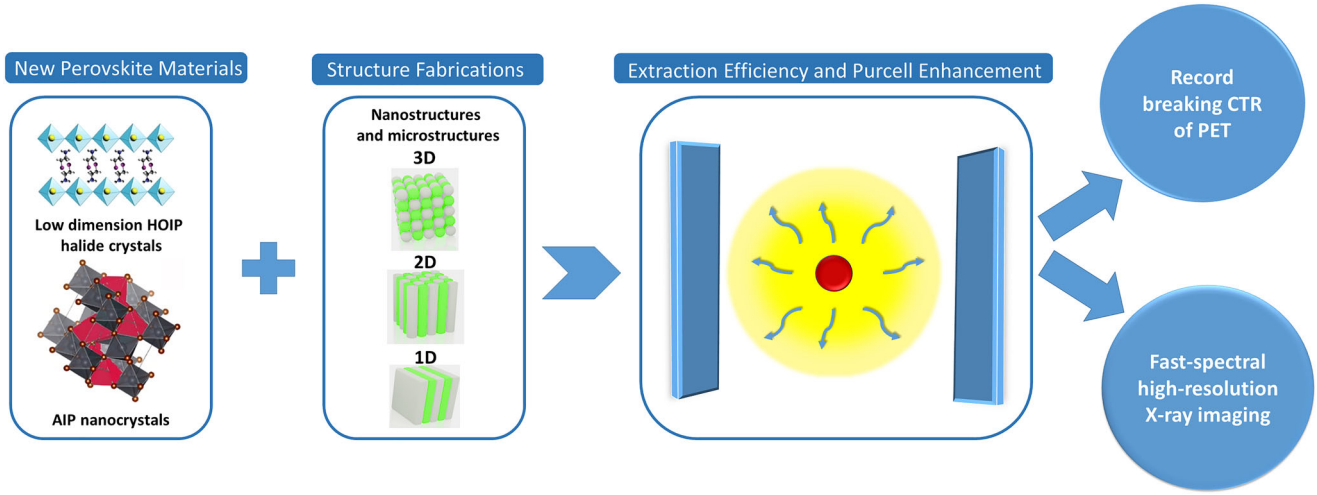

Fig. 4 Research roadmap of high light-yield and fast perovskite scintillators. New perovskite materials with state-of-the-art photonic nanostructures will help to revolutionize PET and fast-spectral high-resolution X-ray imaging.

nanophotonic integration of any presently candidate of perovskite scintillators (two-dimensional HOIP crystals and all-inorganic perovskites nanocrystals) towards high-performance scintillators.

Several material and fabrication challenges may implicate the complexity in this subject and the limitation for searching new materials is raised due to the large offset of the experimental findings with the theoretical parameters. Thus, one may consider overcoming by designing new emergent combined perovskite scintillator materials with the Purcell effect to stimulate spontaneous emission by manipulating the local photonic density of states. The proposed roadmap to tackle the issue is presented in Fig. 4. Recent observation of Purcell-enhanced emission intensity in nanostructure photonics has not been fully coherent with its fast lifetime, and this currently an open target that requires further contemplation. The foundation is to utilize the structure-properties material design to be in line the Purcell-enhanced perovskite photonic crystals upon excited by the high-energy X-ray or gamma-ray irradiation. This essentially requires an elegant approach to find a feasible perovskite structure that simultaneously thin enough for ionized electrons and emitted photons to be confined efficiently without sacrificing its potential scintillation applications. Therefore, such technology will enable a new revolution of imaging and timing for medical, security, and high-energy physics applications such as fast-spectral high-resolution X-ray imaging, >30Mcps/pixel OCR in PCCT, and <30 ps breaking record CTR PET[3,17].

Received: 29 August 2022; Accepted: 1 March 2023;
Published online: 13 March 2023

References

1. Moseley, O. D. I., Doherty, T. A. S., Parmee, R., Anaya, M. & Stranks, S. D. Halide perovskites scintillators: Unique promise and current limitations. *J. Mater. Chem. C* **9**, 11588–11604 (2021).
2. Jana, A. et al. Perovskite: Scintillators, direct detectors, and X-ray imagers. *Mater. Today* **55**, 110–136 (2022).
3. Dujardin, C. et al. Needs, trends, and advances in inorganic scintillators. *IEEE Trans. Nucl. Sci.* **65**, 1977–1997 (2018).
4. Vaněček, V. et al. Advanced halide scintillators: From the bulk to nano. *Adv. Photonics Res.* **3**, 2200011 (2022).
5. Zhu, W. et al. Low-dose real-time X-ray imaging with nontoxic double perovskite scintillators. *Light Sci. Appl.* **9**, 112 (2020).
6. Ryzhikov, V. D. et al. Multi-layer fast neutron detectors based on composite heavy-oxide scintillators for detection of illegal nuclear materials. *Nucl. Instrum. Methods Phys. Res. Sect. A* **903**, 287–296 (2018).
7. Hu, C. et al. LuAG ceramic scintillators for future HEP experiments. *Nucl. Instrum. Methods Phys. Res. Sect. A* **954**, 161723 (2020).
8. Yuan, D. et al. Directional control and enhancement of light output of scintillators by using microlens arrays. *ACS Appl. Mater. Interfaces* **12**, 29473–29480 (2020).
9. Yanagida, T. et al. Temperature dependence of scintillation properties of bright oxide scintillators for well-logging. *Jpn. J. Appl. Phys.* **52**, 076401 (2013).
10. Zhang, Z. et al. Application of liquid scintillators as energy conversion materials in nuclear batteries. *Sens. Actuators A: Phys.* **290**, 162–171 (2019).
11. Combes, C. M., Dorenbos, P., van Eijk, C. W. E., Krämer, K. W. & Güdel, H. U. Optical and scintillation properties of pure and Ce^{3+}-doped Cs_2LiYCl_6 and $Li_3YCl_6:Ce^{3+}$ crystals. *J. Lumin.* **82**, 299–305 (1999).
12. Lempicki, A. & Glodo, J. Ce-doped scintillators: LSO and LuAP. *Nucl. Instrum. Methods Phys. Res. Sect. A* **416**, 333–344 (1998).
13. Shibuya, K., Koshimizu, M., Takeoka, Y. & Asai, K. Scintillation properties of $(C_6H_{13}NH_3)_2PbI_4$: Exciton luminescence of an organic/inorganic multiple quantum well structure compound induced by 2.0 MeV protons. *Nucl. Instrum. Methods Phys. Res. Sect. B* **194**, 207–212 (2002).
14. Birowosuto, M. D. et al. X-ray scintillation in lead halide perovskite crystals. *Sci. Rep.* **6**, 37254 (2016). **The breakthrough report on the development of perovskites-based X-ray scintillators.**
15. Chen, Q. et al. All-inorganic perovskite nanocrystal scintillators. *Nature* **561**, 88–93 (2018).
16. Xie, A. et al. Library of two-dimensional hybrid lead halide perovskite scintillator crystals. *Chem. Mater.* **32**, 8530–8539 (2020).
17. Schaart, D. R., Ziegler, S. & Zaidi, H. Achieving 10 ps coincidence time resolution in TOF-PET is an impossible dream. *Med. Phys.* **47**, 2721–2724 (2020).
18. Cala', R. et al. Sub-100-picosecond time resolution from undoped and Li-doped two-dimensional perovskite scintillators. *Appl. Phys. Lett.* **120**, 241901 (2022). **The impact of lithium dopant to improve the coincidence time resolution of hybrid perovskite scintillators from 100 to 84 ps.**
19. Zhang, Z. et al. Single-crystalline perovskite nanowire arrays for stable X-ray scintillators with micrometer spatial resolution. *ACS Appl. Nano Mater.* **5**, 881–889 (2022).
20. Han, K. et al. Seed-crystal-induced cold sintering toward metal halide transparent ceramic scintillators. *Adv. Mater.* **34**, 2110420 (2022).
21. Dorenbos, P. The quest for high-resolution γ-ray scintillators. *Opt. Mater.: X* **1**, 100021 (2019).
22. Maddalena, F. et al. Inorganic, organic, and perovskite halides with nanotechnology for high–light yield X- and γ-ray scintillators. *Crystals* **9**, 88 (2019).
23. Wu, Y. et al. Zero-dimensional Cs_4EuX_6 (X = Br, I) all-inorganic perovskite single crystals for gamma-ray spectroscopy. *J. Mater. Chem. C* **6**, 6647–6655 (2018).
24. Stand, L. et al. Crystal growth and scintillation properties of Eu^{2+} doped Cs_4CaI_6 and Cs_4SrI_6. *J. Cryst. Growth* **486**, 162–168 (2018).

25. Yang, B. et al. Lead-free halide Rb_2CuBr_3 as sensitive X-ray scintillator. *Adv. Mater.* **31**, 1904711 (2019). **A promising one-dimensional all-inorganic perovskites with strong carrier confinement and near-unity photoluminescence quantum yield (98.6%).**
26. Wei, J.-H. et al. All-inorganic lead-free heterometallic $Cs_4MnBi_2Cl_{12}$ perovskite single crystal with highly efficient orange emission. *Matter* **3**, 892–903 (2020).
27. Kumar, S. et al. Efficient blue electroluminescence using quantum-confined two-dimensional perovskites. *ACS Nano* **10**, 9720–9729 (2016).
28. Xie, A. et al. Lithium-doped two-dimensional perovskite scintillator for wide-range radiation detection. *Commun. Mater.* **1**, 37 (2020). **An implication of lithium doping on the $(PEA)_2PbBr_4$ with a promising fast decay time of 11 ns (80%).**
29. Grancini, G. et al. One-Year stable perovskite solar cells by 2D/3D interface engineering. *Nat. Commun.* **8**, 1–8 (2017).
30. Chen, H., Li, Y. & Xue, D. 2D organic–inorganic hybrid perovskite quantum well materials and their dramatical X-ray optoelectronic properties. *Materials* **14**, 5539 (2021).
31. Even, J., Pedesseau, L. & Katan, C. Understanding quantum confinement of charge carriers in layered 2D hybrid perovskites. *ChemPhysChem* **15**, 3733–3741 (2014).
32. Umebayashi, T., Asai, K., Kondo, T. & Nakao, A. Electronic structures of lead iodide based low-dimensional crystals. *Phys. Rev. B.* **67**, 155405 (2003).
33. Saparov, B. & Mitzi, D. B. Organic–inorganic perovskites: Structural versatility for functional materials design. *Chem. Rev.* **116**, 4558–4596 (2016).
34. Shibuya, K. et al. Development of ultra-fast semiconducting scintillators using quantum confinement effect. *Jpn. J. Appl. Phys.* **43**, L1333 (2004).
35. Panwar, S. et al. Characterization of a Sr co-doped $LaBr_3$:(Ce) detector for γ-ray spectroscopy. *Nucl. Instrum. Methods Phys. Res., Sect. A* **982**, 164567 (2020).
36. Shirwadkar, U. et al. Thallium-based scintillators for high-resolution gamma-ray spectroscopy: Ce^{3+}-doped Tl_2LaCl_5 and Tl_2LaBr_5. *Nucl. Instrum. Methods Phys. Res., Sect. A* **962**, 163684 (2020).
37. Kishimoto, S. et al. Sub-nanosecond time-resolved X-ray measurements using an organic-inorganic perovskite scintillator. *Appl. Phys. Lett.* **93**, 261901 (2008).
38. Cortecchia, D. et al. Polaron self-localization in white-light emitting hybrid perovskites. *J. Mater. Chem. C* **5**, 2771–2780 (2017).
39. Maddalena, F. et al. Effect of commensurate lithium doping on the scintillation of two-dimensional perovskite crystals. *J. Mater. Chem. C* **9**, 2504–2512 (2021).
40. Ohashi, Y., Yasui, N., Yokota, Y., Yoshikawa, A. & Den, T. Submicron-diameter phase-separated scintillator fibers for high-resolution X-ray imaging. *Appl. Phys. Lett.* **102**, 051907 (2013).
41. Datta, A., Fiala, J. & Motakef, S. 2D perovskite-based high spatial resolution X-ray detectors. *Sci. Rep.* **11**, 22897 (2021).
42. Birowosuto, M. D. et al. Thermal-neutron scintillator: Ce^{3+} activated Rb_2LiYBr_6. *J. Appl. Phys.* **101**, 066107 (2007).
43. Bessiere, A., Dorenbos, P., van Eijk, C., Kramer, K. & Gudel, H. New thermal neutron scintillators: Cs_2LiYCl_6: Ce^{3+} and Cs_2LiYBr_6: Ce^{3+}. *IEEE Trans. Nucl. Sci.* **51**, 2970–2972 (2004).
44. Létant, S. E. & Wang, T. F. Semiconductor quantum dot scintillation under γ-ray irradiation. *Nano Lett.* **6**, 2877–2880 (2006).
45. Onoda, D. et al. Development of $(C_6H_5C_2H_4NH_3)_2Pb_{1-x}Cd_xBr_4$ crystal scintillators with two-dimensional quantum-well structures. *J. Lumin.* **237**, 118157 (2021).
46. Cheng, S. et al. Zero-dimensional $Cs_3Cu_2I_5$ perovskite single crystal as sensitive X-ray and γ-ray scintillator. *Phys. Status Solidi Rapid Res. Lett.* **14**, 2000374 (2020).
47. Wang, Q. et al. Highly resolved X-ray imaging enabled by In (I) doped perovskite-like $Cs_3Cu_2I_5$ single crystal scintillator. *Adv. Opt. Mater.* **10**, 2200304 (2022). **In(I) doped perovskite with excellent X-ray detection limit of 96.2 nGy_{air} s^{-1}, and a superior scintillation yield of 53 000 photons per MeV.** https://doi.org/10.1002/adom.202200304.
48. Wang, Q. et al. Achieving efficient neutron and gamma discrimination in a highly stable ^{6}Li-Loaded $Cs_3Cu_2I_5$ perovskite scintillator. *J. Phys. Chem. Lett.* **13**, 9066–9071 (2022).
49. Zhu, Z. et al. Enhanced light extraction of scintillator using large-area photonic crystal structures fabricated by soft-X-ray interference lithography. *Appl. Phys. Lett.* **106**, 241901 (2015).
50. Gupta, S. K. & Mao, Y. Recent advances, challenges, and opportunities of inorganic nanoscintillators. *Front. Optoelectron.* **13**, 156–187 (2020).
51. Protesescu, L. et al. Nanocrystals of cesium lead halide perovskites ($CsPbX_3$, X=Cl, Br, and I): novel optoelectronic materials showing bright emission with wide color gamut. *Nano Lett.* **15**, 3692–3696 (2015).
52. Hormozan, Y., Sychugov, I. & Linnros, J. High-resolution X-ray imaging using a structured scintillator. *Med. Phys.* **43**, 696–701 (2016).
53. Maddalena, F. et al. Stable and bright commercial $CsPbBr_3$ quantum dot-resin layers for apparent X-ray imaging screen. *ACS Appl. Mater. Interfaces* **13**, 59450–59459 (2021).
54. Maddalena, F. et al. Deterministic light yield, fast scintillation, and microcolumn structures in lead halide perovskite nanocrystals. *J. Phys. Chem. C* **125**, 14082–14088 (2021).
55. Zhou, Y., Chen, J., Bakr, O. M. & Mohammed, O. F. Metal halide perovskites for X-ray imaging scintillators and detectors. *ACS Energy Lett.* **6**, 739–768 (2021).
56. Zhou, F. et al. Halide perovskite, a potential scintillator for X-ray detection. *Small Methods* **4**, 2000506 (2020).
57. Lian, L. et al. Efficient and reabsorption-free radioluminescence in $Cs_3Cu_2I_5$ nanocrystals with self-trapped excitons. *Adv. Sci.* **7**, 2000195 (2020).
58. Zhou, Y. et al. Large-area perovskite-related copper halide film for high-resolution flexible X-ray imaging scintillation screens. *ACS Energy Lett.* **7**, 844–846 (2022).
59. Ryu, I. et al. In vivo plain X-ray imaging of cancer using perovskite quantum dot scintillators. *Adv. Funct. Mater.* **31**, 2102334 (2021).
60. Roques-Carmes, C. et al. A framework for scintillation in nanophotonics. *Science* **375**, eabm9293 (2022). **A demonstration on the nanophotonic structures with the ability to shape the spectral, angular, and polarization characteristics of scintillation.**
61. Wang, C. et al. X-ray excited $CsPb(Cl, Br)_3$ perovskite quantum dots-glass composite with long-lifetime. *J. Eur. Ceram. Soc.* **40**, 2234–2238 (2020).
62. Cao, F. et al. Shining emitter in a stable host: design of halide perovskite scintillators for X-ray imaging from commercial concept. *ACS Nano* **14**, 5183–5193 (2020).
63. Ren, C. et al. Confinement of all-inorganic perovskite quantum dots assembled in metal–organic frameworks for ultrafast scintillator application. *Nanoscale* **14**, 4216–4224 (2022).
64. Chen, W. et al. All-inorganic perovskite polymer–ceramics for flexible and refreshable X-ray imaging. *Adv. Funct. Mater.* **32**, 2107424 (2022).
65. Williams, R. T., Wolszczak, W. W., Yan, X. & Carroll, D. L. Perovskite quantum-dot-in-host for detection of ionizing radiation. *ACS Nano* **14**, 5161–5169 (2020).
66. Gandini, M. et al. Efficient, fast and reabsorption-free perovskite nanocrystal-based sensitized plastic scintillators. *Nat. Nanotechnol.* **15**, 462–468 (2020).
67. Salomoni, M., Pots, R., Auffray, E. & Lecoq, P. Enhancing light extraction of inorganic scintillators using photonic crystals. *Crystals* **8**, 78 (2018).
68. Knapitsch, A. et al. Photonic crystals: A novel approach to enhance the light output of scintillation based detectors. *Nucl. Instrum. Methods Phys. Res., Sect. A* **628**, 385–388 (2011).
69. Knapitsch, A. et al. Results of photonic crystal enhanced light extraction on heavy inorganic scintillators. *IEEE Trans. Nucl. Sci.* **59**, 2334–2339 (2012).
70. Kurman, Y., Shultzman, A., Segal, O., Pick, A. & Kaminer, I. Photonic-crystal scintillators: Molding the flow of light to enhance X-ray and γ-ray detection. *Phys. Rev. Lett.* **125**, 040801 (2020).
71. Vahala, K. J. Optical microcavities. *Nature* **424**, 839–846 (2003).
72. Ye, W., Bizarri, G., Birowosuto, M. D. & Wong, L. J. Enhancing large-area scintillator detection with photonic crystal cavities. *ACS Photonics* **9**, 3917–3925 (2022).
73. Hou, S. et al. Concurrent inhibition and redistribution of spontaneous emission from all inorganic perovskite photonic crystals. *ACS Photonics* **6**, 1331–1337 (2019).
74. Klein, M. et al. Polarization-tunable perovskite light-emitting metatransistor. *Adv. Mater.* **35**, 2207317 https://doi.org/10.1002/adma.202207317 (2022).
75. Long, G. et al. Perovskite metasurfaces with large superstructural chirality. *Nat. Commun.* **13**, 1–8 (2022).
76. Tian, J. et al. Optical rashba effect in a light-emitting perovskite metasurface. *Adv. Mater.* **34**, 2109157 (2022).
77. Alekhin, M. S., Biner, D. A., Krämer, K. W. & Dorenbos, P. Improvement of $LaBr_3$:5%Ce scintillation properties by Li^+, Na^+, Mg^{2+}, Ca^{2+}, Sr^{2+}, and Ba^{2+} co-doping. *J. Appl. Phys.* **113**, 224904 (2013).
78. Schmall, J. P. et al. Timing and energy resolution of new near-UV SiPMs coupled to $LaBr_3$:Ce for TOF-PET. *IEEE Trans. Nucl. Sci.* **61**, 2426–2432 (2014).
79. Bhandari, H. B. et al. Large-area crystalline microcolumnar $LaBr_3$:Ce for high-resolution gamma ray imaging. *IEEE Trans. Nucl. Sci.* **60**, 3–8 (2012).

Acknowledgements

We would like to acknowledge the funding provided by the Basic Research Fund 2022 scheme from the Indonesian Ministry for Education, Culture, Research and Technology (303/IT1.B07.1/SPP-LPPM/V/2022) and starting fund from Lukasiewicz Research Network-PORT.

Author contributions

A.W., L.J.D., M.B.A., M.A.M., Md. A.K.S. wrote the manuscript with the help of A.A., S.Z. and L.J.W., M.D.B. finalized the writing and supervised the project.

Competing interests

The authors declare no competing interests.

Additional information

Supplementary information The online version contains supplementary material available at https://doi.org/10.1038/s43246-023-00348-5.

Correspondence and requests for materials should be addressed to Muhammad Danang Birowosuto.

Peer review information *Communications Materials* thanks Yihui He and the other, anonymous, reviewer(s) for their contribution to the peer review of this work. Primary Handling Editor: Aldo Isidori. Peer reviewer reports are available.

Reprints and permission information is available at http://www.nature.com/reprints

Publisher's note Springer Nature remains neutral with regard to jurisdictional claims in published maps and institutional affiliations.